Chemical Plume Tracing using an AUV based on POMDP Source Mapping and A-star Path Planning

Lingxiao Wang
DEPT. OF ELECTRICAL, COMPUTER, SOFTWARE AND SYSTEMS ENG.
Embry-Riddle Aeronautical University
Daytona Beach, FL, 32114.
lingxiaw@my.erau.edu

Shuo Pang
DEPT. OF ELECTRICAL, COMPUTER, SOFTWARE AND SYSTEMS ENG.
Embry-Riddle Aeronautical University
Daytona Beach, FL, 32114.
pang2d8@erau.edu

***Abstract*—This paper presents an engineering-based chemical plume tracing (CPT) method for using on an autonomous underwater vehicle (AUV) to locate a chemical source in an underwater environment with obstacles. Fundamental steps of the proposed method are twofold. Firstly, the estimated source location is obtained by a source likelihood map, which is generated based on a partially observable Markov decision process (POMDP). Secondly, after the estimated source location is determined, the A-star path planning algorithm is used to generate the shortest path toward the target while avoiding obstacles. Simulation results validate the proposed method in environments with either laminar or turbulent flow conditions. Comparing with other chemical source mapping algorithms, such as the hidden Markov model (HMM) based method, the POMDP-based source mapping algorithm converges to the correct chemical source location in a faster rate. Besides, the A-star path planning algorithm enables the AUV to avoid obstacles and the local minima issue in the traditional path planning algorithm, such as the artificial potential field.**

***Index Terms*—Chemical Plume Tracing, Partially observable Markov decision process, autonomous underwater vehicle, A-star path planning**

I. Introduction

Autonomous underwater vehicles (AUVs) are versatile and play an important role in marine surveys [1]. Some surveys, e.g., locating underwater hydrothermal vents, require AUVs with chemical sensing abilities to trace chemical plumes and find chemical sources. The procedure of tracing chemical plumes is termed chemical plume tracing (CPT), which is a significant and essential step in a chemical source localization (CSL) mission.

The most straightforward CPT strategy is the chemotaxis method [2], which commands the robot to move along the gradient of the plume concentration. A common implementation of this method is to install a pair of chemical sensors on the left and right side of a robot, and the robot is commanded to steer toward the side with the higher concentration [3]. Many experiments [4]–[7] have proved that the chemotaxis method is effective when the odor source is placed in a very weak or no turbulent (i.e., low Reynolds numbers) environment, where the plume concentration is a smooth and stable signal.

However, the chemotaxis method is not feasible if an odor source is placed in a turbulent environment, where plumes are conjugated into packets and the plume concentration is an intermittent and patchy signal [8]. In that case, the chemotaxis method often misleads a robot to wrong source locations. To solve this problem, the anemotaxis method, which is inspired by mate-seeking behaviors of male moths, was proposed [9]. A male moth could successfully locate a female moth by tracking pheromones emitted by the female over a long distance [10], [11] and even overcoming obstacles on the way such as forests [12]. To complete this task, a male moth will fly upwind (surge) when detects pheromone plumes and traverse the wind (casting) if pheromone plumes are absent. Li et al. [13] implemented the anemotaxis method on an AUV to search for an underwater chemical source. An adaptive mission planner (AMP) inspired by the 'surge/casting' model in the anemotaxis method was designed to mimic moth behaviors. In the surge behavior, the AUV was commanded to move upflow when it was in the plume, and when it left the plume, it steered an offset angle to change its heading and moved forward for a while. If the AUV re-contacted the plume, it went back to the surge behavior; otherwise, it performed the casting behavior. Results from water experiments [14]–[16] showed that the AUV could successfully locate the chemical source by implementing the anemotaxis method.

Another type of CPT strategies is the engineering-based method, which estimates source locations by generating a source likelihood map and guides the robot toward the estimated location (i.e., the area with the highest probability of containing the chemical source) with path planning algorithms. Methods that produce a source likelihood map are various. For instance, Pang and Farrell [17] proposed an algorithm to calculate probabilities of the plume detection and non-detection events based on a Gaussian plume model, and these probabilities were fused by a Bayesian-based method to iteratively update the source likelihood map. Other numerical algorithms and models were also feasible to recursively update the source likelihood map, such as the particle filter [18], the hidden Markov model (HMM) [19], and the model of a partially observable Markov decision process (POMDP) [20]. After obtaining a source likelihood map, a path planning algorithm that guides the robot moving toward the target is necessary. Pang and Zhu [21] proposed a path planning

algorithm based on the artificial potential field, which directs the robot moving to the area with the highest probability of containing the odor source. In this method, the local minima issue, i.e., the robot is trapped when the attractive force equals to the repulsive force and with the opposite direction, was avoided since there were no obstacles in the search area. Li et al. [22] proposed a route planning method based on the estimated plume trajectories. This method first estimates trajectories of plumes based on a Gaussian plume diffusion model, and then the robot is commanded to move to the area where thick plumes exist. Vergassola, Villermaux, and Shraiman [23] presented the 'infotaxis' method, which utilized information entropies to guide the robot searching for an odor source. The robot is commanded to move toward the direction that mostly reduces the information uncertainty. Experiment results show that the robot trajectory in this method is similar to the anemotaxis method.

In this paper, we present an engineering-based CPT strategy that combines the POMDP-based chemical source mapping and the A-star path planning algorithms. The framework of a POMDP is suitable to model a CSL mission: the AUV (agent) does not know the location of the chemical source, but it can estimate the source location through detection events. We define the hidden state space as the source location, which is implicit and clouded to the AUV. Belief states, which originally describe the probability of the agent being in a state, are adapted to represent the likelihood of the chemical source being located in an area. The estimated source location is selected as the area that has the highest belief state value. After that, the A-star algorithm generates the shortest path from the AUV's current location to the estimated source location while avoiding obstacles. During the course of the AUV following the path, if the source likelihood map updates a new target location, the A-star path planner will re-generate a new path to guide the AUV moving to the new target. The CSL task is considered as successfully completed if the AUV correctly declares the chemical source location.

II. Methodology

A. The Framework of a CSL Mission

It is commonly accepted that a CSL task can be divided into three phases, namely plume finding, plume tracing, and source declaration [24]. Fig. 1 shows the framework of a CSL mission with the proposed CPT strategy. In the first stage, the AUV searches the presence of plumes and tries to get the plume detection in the first time. We adopted a 'zigzag' method proposed in [13] as the initial search strategy. After the AUV detects plumes for the first time, it switches to the second stage: tracing plumes as cues to find the chemical source. The location of the chemical source is estimated using the POMDP-based source mapping algorithm (section II-C) while the path toward the estimated source location is generated by the A-star path planning algorithm (section II-D). After the mapping algorithm converges to an area, the AUV declares the chemical source location and completes the CSL mission.

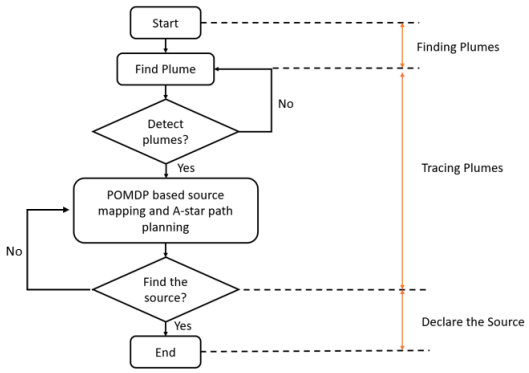

Fig. 1. The framework of a CSL mission with the proposed CPT strategy

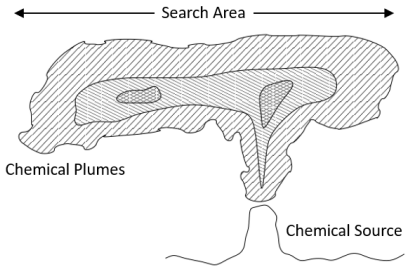

Fig. 2. Chemical plumes in an underwater environment

B. The Simplified Search Area

As shown in Fig. 2, in an underwater environment, chemical plumes mainly disperse at a certain level due to the buoyancy [14]. Thus, the underwater CSL mission could be considered as a two-dimensional (2-D) searching problem. In the project, the search area is simplified as a 2-D rectangular grid, which has m segments in the horizontal direction and n segments in the vertical direction. Fig. 3 shows the proposed search area. A vector $\mathbf{C} = [C_1, C_2, C_3, ..., C_{mn}]$ is used to store positions of cells. It can also be used to represent AUV positions: when the AUV enters a cell, its position is approximated by the cell that it is occupied.

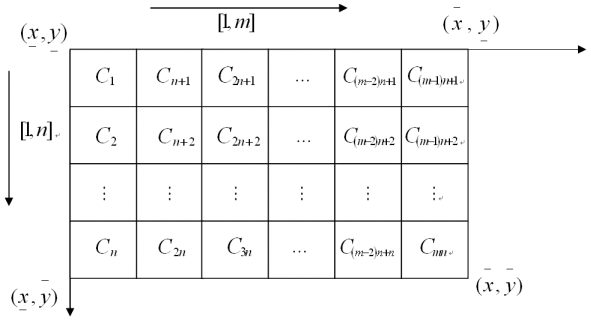

Fig. 3. The simplified search area in the CSL mission

C. The POMDP-based Source Mapping Algorithm

The POMDP-based source mapping algorithm is adopted in this project [20]. A traditional POMDP model [25] is defined by a tuple $(\mathcal{S}, \mathcal{A}, \Omega, P, O, r, b_0)$ as shown below:

- $\mathcal{S}$ is a state space;
- $\mathcal{A}$ is an action space;
- Ω is an observation space;
- P are transition probabilities between states;
- O are observation probabilities;
- r is a reward function defined on the transitions;
- b_0 is an initial probability distribution over states.

In this project, AUV's actions are determined by the path planning algorithm, thus, action related parameters, i.e., reward functions r and the action space $\mathcal{A}$, are redundant. The remainder of this section illustrates a method of adapting each element in a POMDP model into a CSL mission in order to generate a source likelihood map.

1) State Space: States in a traditional POMDP model are hidden to the agent, i.e., the agent does not know which state it is in. In a CSL mission, the AUV does not know the actual chemical source location. Thus, we defined the state space $\mathcal{S}$ as a Boolean vector $\boldsymbol{c} = [c_1, c_2, ..., c_{mn}]$, which stores the information of whether or not a cell containing a chemical source: if a cell has a source, the corresponding Boolean value of the cell in $\boldsymbol{c}$ is 1; otherwise, it is 0.

2) Observation Space and Probabilities: When the AUV enters a cell C_j, it could detect or not detect chemical plumes. Therefore, we defined two events in the observation space $\Omega = \{d, \bar{d}\}$, namely plume detection d and plume non-detection $\bar{d}$. To calculate the probability of the AUV detecting or not detecting chemical plumes, i.e., the observation probabilities O of two observation events, we first assume that the chemical source continuously releases plumes in the water with a constant rate. Second, the AUV only records flow measurements h time units ahead, i.e, if the current time is t_k, the available flow record history is from $t_k - h$ to t_k. Then, the probability of the AUV detecting plumes in a cell C_j at the current time t_k due to a single chemical filament release in a cell C_i at time t_l is defined as [17]:

$$p_{ij}(t_l, t_k) = \frac{L_x L_y}{2\pi(t_k - t_l)\sigma_x\sigma_y} e^{-\frac{\delta_{ix}(t_l,t_k)^2}{2(t_k-t_l)\sigma_x^2}} e^{-\frac{\delta_{iy}(t_l,t_k)^2}{2(t_k-t_l)\sigma_y^2}}, \quad (1)$$

where $[\sigma_x, \sigma_y]$ stands for the natural plume diffusion distances on x and y directions without external flows; $\delta_{ix}(t_l, t_k) = C_{jx} - C_{ix} - s_x(t_l, t_k)$ and $\delta_{iy}(t_l, t_k) = C_{jy} - C_{iy} - s_y(t_l, t_k)$ represent the difference between the distance from the AUV's cell C_j to the estimated source cell C_i and the distance of the odor filament advection caused by the flow $([s_x(t_l, t_k), s_y(t_l, t_k)])$; L_x and L_y are length and width of a cell respectively. Let μ donate the probability of the AUV successfully detecting plumes given that there are detectable plumes at the chemical sensor position, the probability of the AUV detecting plumes in cell C_j at time t_k due to a single chemical filament release can be represented as $\mu p_{ij}(t_l, t_k)$. Since the plume detection and non-detection events are complementary, the probability of the AUV not detecting plumes is $1 - \mu p_{ij}(t_l, t_k)$. Based on our first assumption, the probability of the AUV not detecting plumes in cell C_j if the source continually releases plumes from time t_f to the current time t_k is expressed as:

$$\gamma_{ij}(t_f, t_k) = \prod_{l=f}^{k-1} [1 - \mu p_{ij}(t_l, t_k)], \quad (2)$$

where t_f can be expressed as $t_f = \max(0, t_k - h + 1)$. After the probability of plume non-detection is determined, the probability of detecting plumes in a cell C_j at time t_k, i.e., the probability of plume detection, is expressed as $1 - \gamma_{ij}(t_f, t_k)$.

In summary, observation probabilities of plume detection (d) and plume non-detection ($\bar{d}$) events are presented as below:

$$O(c_j, o_k) = \begin{cases} 1 - \gamma_{ij}(t_f, t_k) & o_k = d \\ \gamma_{ij}(t_f, t_k) & o_k = \bar{d} \end{cases}. \quad (3)$$

3) State Transition Probability: The location of the chemical source in the search area is static in our project. Therefore, the hidden state $\boldsymbol{c}$ is also static. If the source location is in a cell C_i, the transition probability can be expressed as:

$$P(c_i'|c_i) = \begin{cases} 1 & c_i' = c_i \\ 0 & c_i' \neq c_i \end{cases}. \quad (4)$$

where c_i' is the new state.

4) Belief States: In a traditional POMDP model, a belief state $b(s)$ is the probability of the agent being in a state s. In the domain of a CSL mission, a belief state is interpreted as the likelihood of the AUV believes that there is a chemical source in a cell. The updating law for a belief state in an original POMDP model is defined as [26]:

$$b(s') = \frac{O(a, s, o) \sum_{s \in S} P(s'|s, a) b(s)}{\sum_{s \in S} \sum_{s' \in S} O(a, s', o) P(s'|s, a) b(s)}, \quad (5)$$

where s' is the new state after the agent performs the action a; $O(a, s, o)$ is the observation probability; $P(s'|s, a)$ stands for the state transition probability. Combine Eqn. 3, Eqn. 4, and Eqn. 5, we get:

$$b(c_i') = \begin{cases} \dfrac{(1 - \gamma_{ij}(t_f, t_k)) b(c_i)}{\sum_{i=1}^{mn} (1 - \gamma_{ij}(t_f, t_k)) b(c_i)} & o_k = d \\ \dfrac{\gamma_{ij}(t_f, t_k) b(c_i)}{\sum_{i=1}^{mn} \gamma_{ij}(t_f, t_k) b(c_i)} & o_k = \bar{d} \end{cases}. \quad (6)$$

The initial belief state b_0 is defined as $1/mn$ if the AUV does not have the prior information of the source location. Calculating belief states for all cells and putting them on corresponding cell locations in the search area, a source likelihood map is obtained, which can be represented as $[b(c_i)]_{i=1}^{i=mn}$. The estimated source location is the cell that has the highest belief state value, i.e., the cell has the highest probability of containing a chemical source. The location of this cell is passed to the online path planner as a temporary goal until the next belief state update.

D. The A-star based Online Path Planning Algorithm

The A-star algorithm [27] is a widely used path planning method in the process of finding the shortest path in a node-based map. It generates a path between a start and a goal that minimizes the function:

$$f(n) = g(n) + h(n), \tag{7}$$

where $n = (n_x, n_y)$ is a node on the path, $g(n)$ represents the cost of the path from the starting point to a node, and $h(n)$ is the heuristic function from the a node to the goal.

In our application, the search area is divided into mn cells, and each cell is considered as a node. The starting point is the cell that the AUV currently occupies, and the goal is the estimated source location, which is produced from the source likelihood map. The cost function is defined as:

$$g(n) = \begin{cases} 1000 & n \in \bar{B} \\ 0 & n \in B \end{cases}, \tag{8}$$

where $\bar{B}$ is the set of cells that are defined as obstacles, and B is a set of other cells. Note that, $\bar{B} \cup B$ comprises the whole search area. The heuristic function is defined as the Manhattan distance [28]:

$$h(n) = |n_x - G_x| + |n_y - G_y|, \tag{9}$$

where (G_x, G_y) is the coordinate of the goal.

When planning the path, the A-star path planner considers five possible directions, namely left, left-forward, forward, right-forward, and right. The output of the path planner is a series of node (cell) coordinates, which is termed the planned path. Once the source mapping algorithm updates a new estimated source location, the planned path will be updated correspondingly. The AUV follows the planned path until it is updated. The chemical source is declared to be found if the source likelihood map converges, i.e., the estimated source location produced from the source likelihood map does not change over 30 seconds.

III. Simulation Designs

The simulation program, in which the proposed method is evaluated and verified, has three designed components: the search area, AUV dynamics in a 2-D plane, and chemical plumes.

A. Search Area

In the simulation program, the search area is defined as a rectangle with a size of $100 \times 100\ m^2$. It is divided into 1000 cells with 40 segments in the horizontal direction and 25 segments in the vertical direction, and the size of a single cell is $2.5 \times 4\ m^2$. The initial position of the AUV is at $(24, 2)$, and the actual chemical source is located at $(8, 12)$. The obstacle is defined as a rectangular block ($20 \times 7.5\ m^2$), which is placed at the right side and $17.5\ m$ away from the plume source. Fig. 4 shows the designed search area in the simulation program.

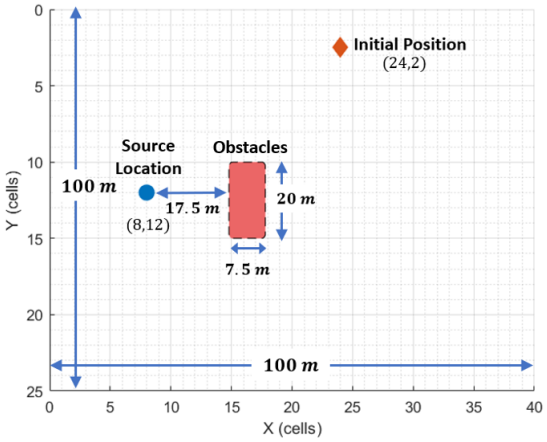

Fig. 4. The designed search area in the simulation program

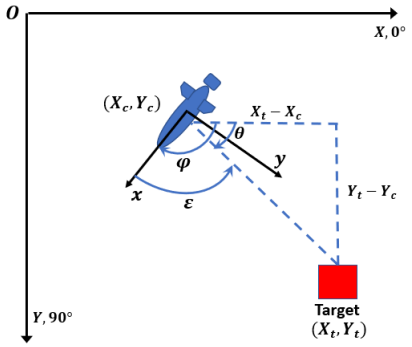

Fig. 5. X and Y forms the global frame; x and y forms the local frame. AUV's heading (φ) is the angle rotating from the X axis to x axis in a clockwise direction. θ is the target heading. ϵ is the heading error, which is calculated by $\epsilon = \varphi - \theta$.

B. AUV Motions Control

Two parameters, headings and velocities, are needed to command an AUV to transport from the current location (X_c, Y_c) to the target (X_t, Y_t) in a horizontal plane. Since the AUV moves in a constant velocity ($2\ m/s$) in the simulation, a target heading is the only variable for controlling an AUV, which can be calculated as:

$$\theta = \arctan\left(\frac{Y_t - Y_c}{X_t - X_c}\right). \tag{10}$$

The AUV rotates to align with the target heading when the AUV's current heading is not equal to it, and the heading error (ϵ) is calculated as the difference between them. Fig. 5 shows the proposed heading control method.

C. Chemical Plume Model

The time-average chemical plume concentration can be calculated based on a a Gaussian plume distribution model [29]:

$$\frac{\overline{C}}{C_{\mathrm{m}}} = \exp\left(\frac{-y^2}{2\sigma_y^2(x, F)}\right), \tag{11}$$

where the mean flow direction is in the x direction, y is the perpendicular distance from the centerline of plumes, $\bar{C}$ and C_m are time-average plume concentration and local centerline concentration respectively, σ_y represents the plume width, which is a function of x position and the flow F. For short-timescale circumstances, the position of the chemical plume advected by flows follows a random walk [17], which can be expressed as:

$$\dot{\mathbf{X}}(t) = \mathbf{U}(\mathbf{X}, t) + \mathbf{N}(t), \tag{12}$$

where $\mathbf{X} = (x, y)$ is the chemical plume location, $\mathbf{U} = (u_x, u_y)$ is the mean flow velocity, and $\mathbf{N}$ is a Gaussian random process with zero mean and (σ_x^2, σ_y^2) variance. By integrating Eqn. 12, the location of the chemical plume $\mathbf{X}(t_k)$ at the current time t_k that was released at time t_s can be expressed as:

$$\mathbf{X}(t_k) = \mathbf{X}(t_s) + \int_{t_s}^{t_k} \mathbf{U}(\mathbf{X}(\tau), \tau) d\tau + \int_{t_s}^{t_k} \mathbf{N}(\tau) d\tau. \tag{13}$$

In simulations, the chemical source is fixed in a constant position and releases $N = 10$ filaments per time unit $d\tau$. Thus, in the time interval $[t_s, t_k]$, there are $N(t_k - t_s)/d\tau$ filaments released with positions denoted by: $P(t_s, t_k) = [\mathbf{X}(t_s), \mathbf{X}(t_s + d\tau/N), \mathbf{X}(t_s + 2d\tau/N), ..., \mathbf{X}(t_k)]$. $d\tau$ is 1 in the simulation program.

IV. Results

The proposed CPT strategy was tested in environments with either laminar or turbulent water flows. To evaluate the performance of the proposed method, we use Bayesian-based and HMM-based source mapping methods as benchmarks.

A. The Environment with Laminar Flows

Fig. 7 shows source likelihood maps generated by the POMDP-based source mapping algorithm at different times when the chemical source is placed in an environment with laminar water flows (mean flow $[u_x, u_y]$: $[1, 0]$ m/s). In the beginning, all cells are initially assigned with a uniform probability ($1/mn = 0.001$) since no information about the source location is known before performing the search process. The AUV follows a 'zigzag' search trajectory [13] to get the initial contact with plumes. Fig. 7(a) reflects the initial phase of the simulation: cells have the uniform probability (around 0.001) in red areas and have the probability of 0 in white areas. This is because white areas are in the up flow direction of the AUV, and since the AUV does not detect plumes, the POMDP-based source mapping algorithm excludes the source location from these areas, i.e., updates their probabilities to 0. After the first plume detection, as shown in Fig. 7(b), the source mapping algorithm narrows the possible source locations down to up flow areas and transmits the cell's location that has the highest probability of containing the chemical source to the A-star path planner, who generates the shortest path from the AUV's current location to the estimated target while avoiding obstacles. In Fig. 7(d), the AUV correctly finds the source location after three plume detection events. Fig. 7(e)-7(h) present source likelihood maps at different times during the CSL mission.

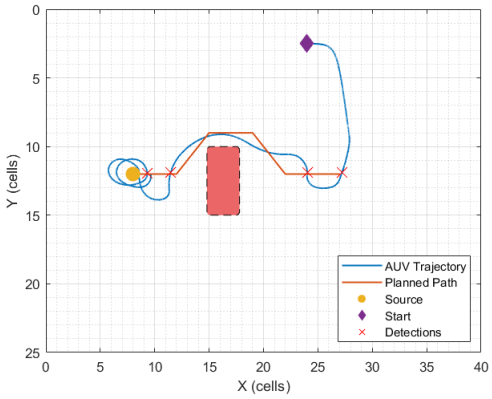

Fig. 6. A summary of the CSL mission reported in Fig. 7. The AUV follows the path generated from the A-star algorithm while tracing the plumes. The AUV correctly finds the source location at the end of the mission.

Since the estimated source location changes when the source likelihood map updates, there are multiple planned paths output from the A-star path planner during the searching procedure. These planned paths are combined together to generated an overall planned path over the entire CSL mission. Fig. 6 presents the overall planned path and the actual trajectory of the AUV in the CSL mission.

B. The Environment with Turbulent Flows

The proposed CPT strategy is also tested in a turbulent environment. The mean flow velocity $[1, 0]$ m/s is added with Gaussian white noises [30]. Thus, flow directions and velocities change unpredictably, which is similar to a real underwater environment. Fig. 8 shows AUV trajectories and source likelihood maps generated by the proposed method at different time steps. At t=42s, the AUV gets the first detection of plumes, and the source likelihood map narrows possible source locations down to up flow areas. At t=53s, after the second detection, the estimated chemical source is located at the up flow areas, which are close to the actual source location. From t=53s to t=80s, the AUV proceeds to the target while avoids obstacles. Eventually, at t=184s, the AUV correctly finds the chemical source location and declares the source location if the estimated source location does not change over 30 seconds. Fig. 9 shows the planned path and the actual AUV trajectory in the experiment reported in Fig. 8.

C. Compare with HMM-Based and Bayesian-Based Source Mapping Methods

We compare the results of the POMDP based source mapping method with the HMM-based [19] and the Bayesian-based [17] source mapping algorithms. Table I shows the result of the comparison. All source mapping methods can correctly converge to the correct chemical source location in environments with either laminar or turbulent water flows, but the POMDP-based source mapping method has a faster rate

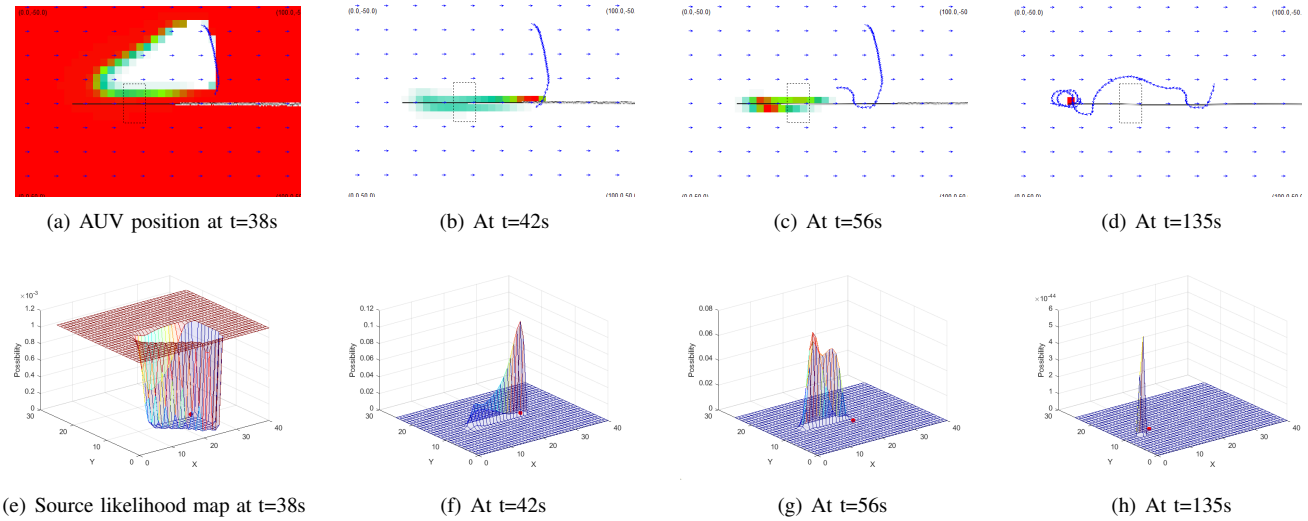

(a) AUV position at t=38s (b) At t=42s (c) At t=56s (d) At t=135s

(e) Source likelihood map at t=38s (f) At t=42s (g) At t=56s (h) At t=135s

Fig. 7. A CSL mission in an environment with laminar flows that blow from the left to right side with a constant velocity 1 m/s. Diagrams in the first row show AUV trajectories at different times, which are indicated by blue curves. Arrays of arrows in the background reflects the flow information: the direction of an arrow points to the flow direction, and the length of an arrow exhibits the flow velocity. The black trail in the horizontal centerline of a diagram is the plume propagation trajectory. The obstacle is represented by a rectangle with dotted lines. Colors in the background reflect the likelihood of a cell containing the chemical source: the darker the color, the higher the probability (red: highest, white: lowest). Diagrams in the second row present source likelihood maps at same time steps with the first row diagrams. The horizontal plane (X and Y) of a source likelihood map has the same size with the search area, and the vertical axis shows the probability of a cell containing a chemical source. The AUV's location is indicated by a red dot on the horizontal plane.

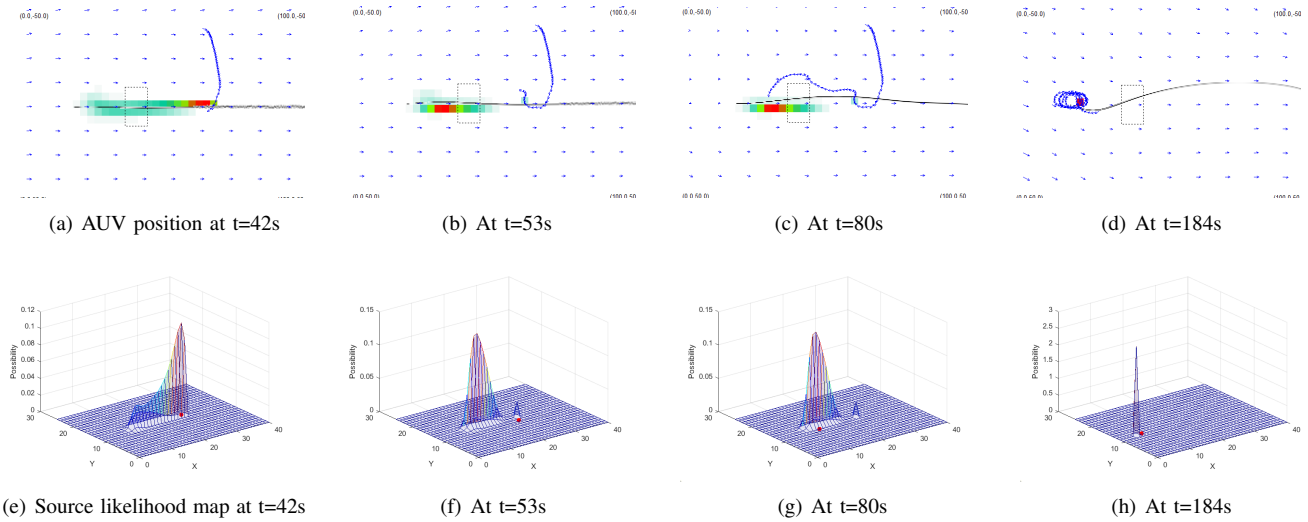

(a) AUV position at t=42s (b) At t=53s (c) At t=80s (d) At t=184s

(e) Source likelihood map at t=42s (f) At t=53s (g) At t=80s (h) At t=184s

Fig. 8. A CSL mission in an environment with turbulent flows. Gaussian white noises were added on flow's velocities. The black trail represents the plume trajectory, which changes unpredictably due to turbulent flows. Diagrams in the first row present AUV trajectories and in the second row are source likelihood maps. Notations of variables and definitions of plots are same with Fig. 7.

of convergence comparing to the HMM-based method. Based on experiment results, the POMDP-based method converges to a correct chemical source location with 135 seconds in the laminar flows environment while the HMM-based method needs 160 seconds. In the turbulent flows environment, the POMDP-based method needs 184 seconds and the HMM-based requires 270 seconds to converge to the correct source location. Comparing to the Bayesian-based source mapping algorithm, the POMDP-based method has a comparable performance in terms of the searching time. This is because both source mapping algorithms employ the same plume detection and non-detection probabilities, but they are differed in the process of fusing probabilities.

TABLE I
THE COMPARISON OF THE POMDP-BASED, HMM-BASED, AND BAYESIAN-BASED SOURCE MAPPING ALGORITHMS

	Searching Time (Seconds) Laminar Flows	Searching Time (Seconds) Turbulent Flows
POMDP-based	135	184
HMM-based	160	270
Bayesian-based	121	140

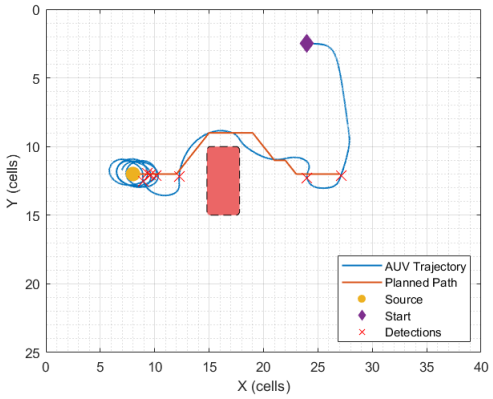

Fig. 9. A summary of the CSL mission reported in Fig. 8. The AUV follows the path generated from the A-star algorithm while tracing the plumes. The AUV correctly finds the source location at the end of the mission.

V. Conclusion

Simulation results show that the POMDP-based source mapping algorithm is valid to estimate the chemical source location in environments with either laminar or turbulent flows. Comparing with HMM-based and Bayesian-based source mapping algorithms, the POMDP-based method has the advantage in the converging rate: it only needs few plume detection events to converge to a correct source location, which is beneficial for saving the search time in a CSL mission. Also, by properly defining a heuristic function, the proposed A-star based online path planning method is feasible to effectively generate the shortest path toward the target while avoiding obstacles. Comparing with the traditional artificial potential field method, the proposed path planner is more effective since it does not have the minia point issue.

References

[1] J. Yuh, G. Marani, and D. R. Blidberg, "Applications of marine robotic vehicles," *Intelligent service robotics*, vol. 4, no. 4, p. 221, 2011.

[2] H. Ishida, K.-i. Suetsugu, T. Nakamoto, and T. Moriizumi, "Study of autonomous mobile sensing system for localization of odor source using gas sensors and anemometric sensors," *Sensors and Actuators A: Physical*, vol. 45, no. 2, pp. 153–157, 1994.

[3] G. Sandini, G. Lucarini, and M. Varoli, "Gradient driven self-organizing systems," in *Proceedings of 1993 IEEE/RSJ International Conference on Intelligent Robots and Systems (IROS'93)*, vol. 1. IEEE, 1993, pp. 429–432.

[4] F. W. Grasso, T. R. Consi, D. C. Mountain, and J. Atema, "Biomimetic robot lobster performs chemo-orientation in turbulence using a pair of spatially separated sensors: Progress and challenges," *Robotics and Autonomous Systems*, vol. 30, no. 1-2, pp. 115–131, 2000.

[5] R. A. Russell, A. Bab-Hadiashar, R. L. Shepherd, and G. G. Wallace, "A comparison of reactive robot chemotaxis algorithms," *Robotics and Autonomous Systems*, vol. 45, no. 2, pp. 83–97, 2003.

[6] A. Lilienthal and T. Duckett, "Experimental analysis of gas-sensitive Braitenberg vehicles," *Advanced Robotics*, vol. 18, no. 8, pp. 817–834, 2004.

[7] H. Ishida, G. Nakayama, T. Nakamoto, and T. Moriizumi, "Controlling a gas/odor plume-tracking robot based on transient responses of gas sensors," *IEEE Sensors Journal*, vol. 5, no. 3, pp. 537–545, 2005.

[8] J. Murlis and C. Jones, "Fine-scale structure of odour plumes in relation to insect orientation to distant pheromone and other attractant sources," *Physiological Entomology*, vol. 6, no. 1, pp. 71–86, 1981.

[9] J. S. Kennedy and D. Marsh, "Pheromone-regulated anemotaxis in flying moths," *Science*, vol. 184, no. 4140, pp. 999–1001, 1974.

[10] R. T. Cardé and M. A. Willis, "Navigational strategies used by insects to find distant, wind-borne sources of odor," *Journal of chemical ecology*, vol. 34, no. 7, pp. 854–866, 2008.

[11] R. T. Cardé and A. Mafra-Neto, "Mechanisms of flight of male moths to pheromone," in *Insect pheromone research*. Springer, 1997, pp. 275–290.

[12] J. Elkinton, C. Schal, T. Onot, and R. Cardé, "Pheromone puff trajectory and upwind flight of male gypsy moths in a forest," *Physiological Entomology*, vol. 12, no. 4, pp. 399–406, 1987.

[13] W. Li, J. A. Farrell, S. Pang, and R. M. Arrieta, "Moth-inspired chemical plume tracing on an autonomous underwater vehicle," *IEEE Transactions on Robotics*, vol. 22, no. 2, pp. 292–307, 2006.

[14] J. A. Farrell, S. Pang, and W. Li, "Chemical plume tracing via an autonomous underwater vehicle," *IEEE Journal of Oceanic Engineering*, vol. 30, no. 2, pp. 428–442, 2005.

[15] W. Li, "Abstraction of odor source declaration algorithm from moth-inspired plume tracing strategies," in *2006 IEEE International Conference on Robotics and Biomimetics*. IEEE, 2006, pp. 1024–1029.

[16] S. Pang, "Development of a guidance system for AUV chemical plume tracing," in *OCEANS 2006*. IEEE, 2006, pp. 1–6.

[17] S. Pang and J. A. Farrell, "Chemical plume source localization," *IEEE Transactions on Systems, Man, and Cybernetics, Part B (Cybernetics)*, vol. 36, no. 5, pp. 1068–1080, 2006.

[18] J.-G. Li, Q.-H. Meng, Y. Wang, and M. Zeng, "Odor source localization using a mobile robot in outdoor airflow environments with a particle filter algorithm," *Autonomous Robots*, vol. 30, no. 3, pp. 281–292, 2011.

[19] J. A. Farrell, S. Pang, and W. Li, "Plume mapping via hidden Markov methods," *IEEE Transactions on Systems, Man, and Cybernetics, Part B (Cybernetics)*, vol. 33, no. 6, pp. 850–863, 2003.

[20] J. Hai-Feng, C. Yu, D. Wei, and P. Shuo, "Underwater chemical plume tracing based on partially observable markov decision process," *International Journal of Advanced Robotic Systems*, vol. 16, no. 2, p. 1729881419831874, 2019.

[21] S. Pang and F. Zhu, "Reactive planning for olfactory-based mobile robots," in *2009 IEEE/RSJ International Conference on Intelligent Robots and Systems*. IEEE, 2009, pp. 4375–4380.

[22] J.-G. Li, M.-L. Cao, and Q.-H. Meng, "Chemical Source Searching by Controlling a Wheeled Mobile Robot to Follow an Online Planned Route in Outdoor Field Environments," *Sensors*, vol. 19, no. 2, p. 426, 2019.

[23] M. Vergassola, E. Villermaux, and B. I. Shraiman, "infotaxis as a strategy for searching without gradients," *Nature*, vol. 445, no. 7126, p. 406, 2007.

[24] G. Kowadlo and R. A. Russell, "Robot odor localization: a taxonomy and survey," *The International Journal of Robotics Research*, vol. 27, no. 8, pp. 869–894, 2008.

[25] O. Sigaud and O. Buffet, *Markov decision processes in artificial intelligence*. John Wiley & Sons, 2013.

[26] M. L. Littman, "A tutorial on partially observable markov decision processes," *Journal of Mathematical Psychology*, vol. 53, no. 3, pp. 119–125, 2009.

[27] P. E. Hart, N. J. Nilsson, and B. Raphael, "A formal basis for the heuristic determination of minimum cost paths," *IEEE transactions on Systems Science and Cybernetics*, vol. 4, no. 2, pp. 100–107, 1968.

[28] D.-J. Chang, A. H. Desoky, M. Ouyang, and E. C. Rouchka, "Compute pairwise manhattan distance and pearson correlation coefficient of data points with gpu," in *2009 10th ACIS International Conference on Software Engineering, Artificial Intelligences, Networking and Parallel/Distributed Computing*. IEEE, 2009, pp. 501–506.

[29] J. P. Crimaldi, M. B. Wiley, and J. R. Koseff, "The relationship between mean and instantaneous structure in turbulent passive scalar plumes," *Journal of Turbulence*, vol. 3, no. 14, pp. 1–24, 2002.

[30] J. A. Farrell, J. Murlis, X. Long, W. Li, and R. T. Cardé, "Filament-based atmospheric dispersion model to achieve short time-scale structure of odor plumes," *Environmental fluid mechanics*, vol. 2, no. 1-2, pp. 143–169, 2002.